Chemical Engineering Journal 108 (2005) 117–125

Chemical Engineering Journal

www.elsevier.com/locate/cej

CFD simulation of steady state heat transfer in bubble columns

Mahesh T. Dhotre, Vivek S. Vitankar, Jyeshtharaj B. Joshi *

Institute of Chemical Technology, Matunga, Mumbai 400019, India

Received 2 September 2004; received in revised form 19 December 2004; accepted 21 January 2005

Abstract

A low Reynolds number k–ε computational fluid dynamics (CFD) model has been used for the description of flow pattern near the wall. An excellent agreement has been shown between the predicted and experimental hold-up and velocity profiles. The CFD model has been extended for the prediction of heat transfer for two-phase gas–liquid flows in bubble columns. A comparison has been presented between the predicted and the experimental data.

Keywords: Bubble columns; Design; CFD; Fluid mechanics; Mathematical modelling; Low Reynolds number model; Heat transfer coefficient

1. Introduction

In bubble columns, the gas phase moves in the form of dispersed bubbles in a continuous liquid phase. The bubble columns operate either in a homogeneous regime or heterogeneous regime. The homogeneous regime is characterized by practically uniform concentration of bubbles throughout the column and no significant bulk convective motion. In contrast, the heterogeneous regime is characterized by the non-uniform bubble concentration (together with wide bubble size distribution) and intense convective motion of the liquid phase. In majority of the commercial installations of bubble columns, heterogeneous regime prevails. A schematic of bubble column (heterogeneous regime) is shown in Fig. 1.

Bubble columns are widely used in commercial practice for a wide range of applications, such as catalytic hydrogenation, air-oxidation, halogenation, hydro-halogenation, ammonolysis, ozonolysis, etc. Though bubble columns are simple in construction, the present design practice is still closer to art than science and most of the design estimates are empirical. For instance, a large number of correlations are available for the axial dispersion coefficient, pressure drop, mass transfer coefficient and heat transfer coefficient, etc., which are empirical or semi-empirical in character. One of the most important drawbacks of such correlations is the range of applicability, in particular, in view of the large variety in the nature of gas–liquid systems (and/or the range of operating conditions), such as Fisher-Tropsch synthesis, column flotation, fermentation, etc.

The root cause for the present status of empiricism has been the complexity of the underlying fluid mechanics. In the majority of cases, the flow is turbulent and the rates of transfer processes cannot be predicted from the first principles. During the past 30 years, there have been continuous and vigorous attempts to gain control over the situation. In particular, developments in computational fluid dynamics (CFD) have accelerated in the past two decades because of the spectacular progress in digital computing. Stewart and Wendroff [1], Jacobson et al. [2] and Joshi [3] have critically reviewed the subject of CFD modeling of bubble columns.

The next step is the development of relationship between the flow pattern and the different design objectives. For instance, the transport phenomena near the wall depend crucially on recognizing and accounting for the role of the turbulent motions adjacent to the wall. Over the years, the near-wall turbulence has been the target of number of numerical and experimental investigations. The presence of wall ensures the molecular viscosity to influence directly the process of production, destruction and transport of turbulence, which in turn affect the other transport processes, such as wall heat and mass transfer. In the past, near-wall turbulence

* Corresponding author. Tel.: +91 22 414 5616; fax: +91 22 414 5614.
E-mail address: jbj@udct.org (J.B. Joshi).

1385-8947/$ – see front matter © 2005 Elsevier B.V. All rights reserved.
doi:10.1016/j.cej.2005.01.006

Nomenclature

A	constant defined as in Eqs. (16) and (20)
C	constant in heat transfer coefficient relations
C_B	interface energy transfer factor
C_0, C_1	drift flux constant
C_P	specific heat capacity of the liquid ($J\,kg^{-1}\,K^{-1}$)
$C_{\varepsilon1}$, $C_{\varepsilon2}$, C_μ	constant in turbulence models
D	column diameter (m)
d_B	bubble size (mm)
E	term in low Reynolds number model
E_T	rate of energy transfer from gas phase to liquid phase (W)
f_1, f_2, f_μ	functions in low Reynolds number model
F_{DZ}	total drag force (N)
Fr	Froude number
g	acceleration due to gravitation ($m\,s^{-2}$)
h_W	heat transfer coefficient ($W\,m^{-2}\,K^{-1}$)
H_D	height of gas dispersion (m)
k	turbulent kinetic energy ($m^2\,s^{-2}$)
k_L	thermal conductivity of the liquid ($W\,K^{-1}$)
k_0	centreline turbulent kinetic energy ($m^2\,s^{-2}$)
L	length of pipe or column (m)
L_c	characteristic heater dimension (m)
p	pressure ($N\,m^{-2}$)
Pr	Prandtl number
q	heat transfer rate ($W\,m^{-2}$)
q_C	heat transfer rate at center ($W\,m^{-2}$)
q_R	heat transfer rate at wall ($W\,m^{-2}$)
r	radial distance (m)
R	radius of column (m)
Re	Reynolds number
R_T	turbulent Reynolds number ($k^2/\nu\varepsilon$)
R_y	turbulent Reynolds number based on y ($yk^{1/2}/\nu$)
St	Stanton number
t_c	contact time (s)
T	temperature (K)
$T(r, z)$	temperature at any radial and axial location (K)
$T(0, z)$	temperature at centre and any axial location (K)
u_L	axial liquid velocity ($m\,s^{-1}$)
u^*	friction velocity ($m\,s^{-1}$)
U_r	radial velocity component ($m\,s^{-1}$)
v	velocity scale ($m\,s^{-1}$)
v_F	eddy velocity ($m\,s^{-1}$)
v_B	volume of a single bubble (m^3)
V_C	circulation velocity ($m\,s^{-1}$)
V_G	superficial gas velocity ($m\,s^{-1}$)
$V_{B,\infty}$	terminal rise velocity of a single bubble ($m\,s^{-1}$)
V_S	slip velocity ($m\,s^{-1}$)
x_1	distance along the wall (m)
x	distance from wall (m)
y	normal distance from the wall, R–r, (m)
y^+	dimensionless wall distance $\left(\frac{y}{v}\sqrt{\frac{2}{3}k_0}\right)$
z	axial distance (m)

Greek symbols

α	thermal diffusivity
α_0	molecular thermal diffusivity
$\bar{\in}_G$	average fractional gas hold up
$\bar{\in}_L$	average fractional liquid hold up
ε	turbulent kinetic energy dissipation rate ($m^2\,s^{-3}$)
μ_L	molecular viscosity ($N\,m^{-2}\,s$)
μ_w	molecular viscosity at the wall ($N\,m^{-2}\,s$)
θ	dimensioned temperature difference
θ^+	dimensionless temperature difference
$\bar{\theta}$	temperature difference
ρ_L	density of liquid ($kg\,m^{-3}$)
ρ_G	density of gas ($kg\,m^{-3}$)
σ	surface tension of the liquid ($N\,m^{-1}$)
σ_ε	Prandtl number for kinetic energy dissipation rate
σ_k	Prandtl number for kinetic energy
ν	molecular kinematic viscosity of liquid ($m^2\,s^{-1}$)
ν_t	turbulent viscosity of liquid ($m^2\,s^{-1}$)

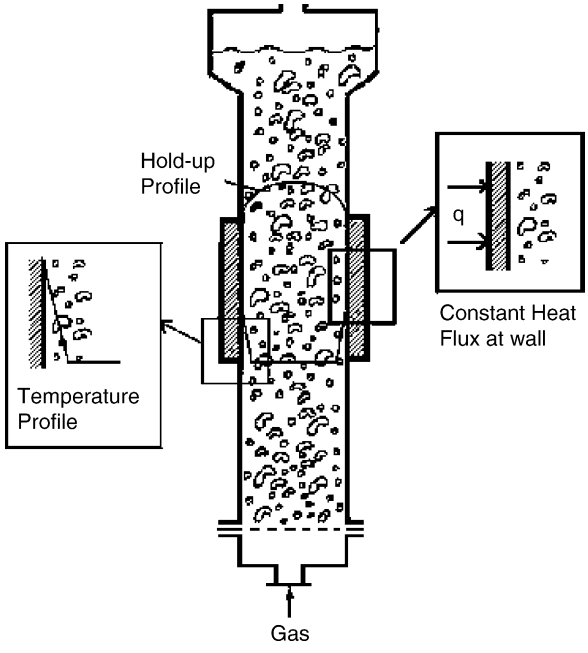

Fig. 1. Schematic figure of the bubble column reactor.

models or low Reynolds number models, which attempt to directly model the influence of molecular viscosity, have been developed. The approach incorporates either a wall damping effect or a direct effect of molecular viscosity, or both, on the empirical constants and functions in the turbulence transport equations. Thakre and Joshi [4] have analyzed the efficacy of 12 different low Reynolds number k–ε models and have recommended Lai and So [5] model (LSO) for the prediction of near-wall flows. Further, Thakre and Joshi [4] extended the flow model for the prediction of heat transfer coefficient in single-phase pipe flows. On the basis of this experience, it was thought desirable to extend a low Reynolds number CFD model for heat transfer in bubble columns.

Bubble columns find wide spread application in highly thermal processes due to their excellent heat transfer properties. In these reactors, the chemical reaction is accompanied by the heat effects and either heat is supplied or removed depending upon the endothermic or the exothermic nature of the reaction. The information on heat transfer coefficient between cooling or heating surface and the gas–liquid dispersed bed is required for designing the bubble columns. In view of this, CFD model has been developed in the present work for prediction of heat transfer coefficient in bubble column.

2. CFD model for flow pattern

The set of governing equations for steady state, incompressible, fully developed two-phase flow in bubble column, in cylindrical coordinate system is represented by the following equations of change:

Momentum equation:

$$-\frac{\rho_L}{r}\frac{\partial}{\partial r}\left(r\in_L(\nu+\nu_t)\frac{\partial u_L}{\partial r}\right) = -\in_L\frac{\partial p}{\partial z} + \in_L g\rho_L + \in_L F_{DZ} \quad (1)$$

$$-\frac{\rho_G}{r}\frac{\partial}{\partial r}\left(r\in_G(\nu+\nu_t)\frac{\partial u_G}{\partial r}\right) = -\in_G\frac{\partial p}{\partial z} + \in_G g\rho_G - \in_L F_{DZ} \quad (2)$$

Turbulent kinetic energy (k) equation:

$$-\frac{1}{r}\frac{\partial}{\partial r}\left(r\in_L\left(\nu+\frac{\nu_t}{\sigma_k}\right)\frac{\partial k}{\partial r}\right) = \nu_t\in_L\left(\frac{\partial u_L}{\partial r}\right)^2 + \in_L C_B F_{DZ} V_S - \varepsilon\in_L \quad (3)$$

Turbulent energy dissipation rate (ε):

$$-\frac{1}{r}\frac{\partial}{\partial r}\left(r\in_L\left(\nu+\frac{\nu_t}{\sigma_\varepsilon}\right)\frac{\partial \varepsilon}{\partial r}\right) = \frac{\in_L\varepsilon}{k}\left[C_{\varepsilon1}f_1\nu_t\left(\frac{\partial u_L}{\partial r}\right)^2 + C_{\varepsilon1}C_B F_{DZ}V_S\right] - \frac{\in_L\varepsilon^2}{k}C_{\varepsilon2}f_2 + E\in_L \quad (4)$$

where

$$\nu_t = C_\mu f_\mu\frac{k^2}{\varepsilon} \quad (5)$$

$$f_1 = 1 + \left[1 - 0.6\exp\left(-\frac{Re}{10^4}\right)\right]\exp\left(-\left(\frac{R_T}{64}\right)^2\right) \quad (6)$$

$$f_2 = 1 - \frac{2}{9}\exp\left[-\left(\frac{R_T}{64}\right)^2\right] \quad (7)$$

$$f_\mu = 1 - \exp(-0.215\ y^+) \quad (8)$$

$$E = 2\nu C_{\varepsilon2}f_2\frac{\varepsilon}{k}\left(\frac{d\sqrt{k}}{dr}\right)^2 + \exp\left(-\left(\frac{R_T}{64}\right)^2\right) \times\left[\left(\frac{7}{9}C_{\varepsilon2}-2\right)\frac{\varepsilon}{k}\left(\varepsilon - 2\nu\left(\frac{d\sqrt{k}}{dr}\right)^2\right) - \frac{1}{2k}\left(\varepsilon - \frac{2\nu k}{y}\right)^2\right] \quad (9)$$

Boundary condition:

$$\text{At centre}\quad \frac{du_L}{dr} = 0;\ \ \frac{du_G}{dr} = 0;\ \ \frac{dk}{dr} = 0;\ \ \frac{d\varepsilon}{dr} = 0$$

$$\text{At wall},\quad k = 0;\ \ \varepsilon = 2\nu\left(\frac{d\sqrt{k}}{dr}\right)^2;\ \ u_L = 0; \quad (10)$$

The LSO model has recommended a value of 0.015 for the constant in the f_μ relation. This value of constant was obtained for the case of single-phase pipe flow. For this purpose, Lai and So [5] had used extensive comparison with the experimental data. Therefore, it is obvious that the same constant is not applicable for a markedly different situation of two-phase flows. The level of turbulence in bubble columns is at much higher level and the boundary layer thickness is much thinner. Therefore, another value of constant is required for the simulations in bubble columns. It must be, however, emphasized that the values of constant so selected [(0.015) by Lai and So [5] and (0.215) in the present case] are selected only once and do not depend upon the column diameter, superficial gas velocity and the physical properties of gas and liquid phases. The values of other constants are $C_\mu = 0.09$, $C_{\varepsilon1} = 1.35$, $C_{\varepsilon2} = 1.8$ and $\sigma_\varepsilon = 1.3$ as suggested by Lai and So [5]. Interfacial forces between gas bubbles and liquid, modeling of pressure gradient and the other related issues have been discussed in Vitankar et al. [6].

3. Interphase energy transfer

The details pertaining to the energy balance have been given by Joshi [3]. The rate of energy transfer from gas to

liquid phase is given by:

$$E_T = \frac{\pi}{4} D^2 (\rho_L - \rho_G) g H_D \bar{\in}_L (V_G + (C_B - 1)\bar{\in}_G V_s) \quad (11)$$

When bubbles rise, the pressure energy is converted into turbulent kinetic energy. A fraction of C_B is considered to get transferred to the liquid phase. The rate of energy given by Eq. (11) is finally dissipated in the turbulent liquid motion. To establish the energy balance, the predicted energy dissipation rate from CFD simulations needs to be equal to the input rate given by Eq. (11).

4. CFD model for heat transfer

As the heat transfer process is completely governed by the flow pattern and thermal diffusivity (eddy diffusivity following Reynolds analogy), correct velocity profile and corresponding diffusivity should yield the heat transfer coefficient. Lin and Wang [7] have observed that the flow and heat transfer is profoundly dominated by the macroscopic hydrodynamics structure. Hence, the velocity profiles and eddy diffusivity obtained by low Reynolds number k–ε model is expected to predict heat transfer coefficient.

4.1. Heat transfer model equation

The following assumptions have been made:

1. The radial variation of eddy diffusivity (ν_t) was obtained from the solution of the Eq. (1)–(10).
2. The heat transfer process has been considered for the case of steady state and constant heat flux.

The steady state heat transfer governing equation is given by:

$$u_L \in_L \frac{\partial T}{\partial z} = \frac{1}{r}\frac{\partial}{\partial r}\left(r \in_L (\alpha + \alpha_0) \frac{\partial T}{\partial r} \right) \quad (12)$$

For the case of constant wall heat flux, radial temperature profiles are well stabilized; so that $T(r,z)$ is a function of r alone, so that the constancy of the wall flux implies that:

$$T(r, z) = \theta I + Az \quad (13)$$

where A is a constant. It is obvious that the sign of A will be positive in the central up flow region and negative in near-wall down-flow area. Substitution of Eq. (13) into Eq. (12) yields an ordinary differential Eq. for θ:

$$\frac{1}{r}\frac{\mathrm{d}}{\mathrm{d}r}\left(r \in_L (\alpha + \alpha_0) \frac{\mathrm{d}\theta}{\mathrm{d}r} \right) = u_L A \in_L \quad (14)$$

above equation can be solved for two different cases:

Case 1. Wall heating

Parameter A in Eq. (14) can be expressed in terms of imposed constant heat flux. Integrating over $r = 0$–R and using the fact that:

$$\frac{\mathrm{d}\theta}{\mathrm{d}r} = 0 \ \text{ at } \ r = 0$$

$$q_R = -C_P \rho_L \in_L \alpha_0 \left(\frac{\mathrm{d}\theta}{\mathrm{d}r} \right)_R \ \text{ at } \ r = R \quad (15)$$

$$A = -\frac{q_R R}{\rho_L C_P \int_0^R u_L \in_L r \mathrm{d}r} \quad (16)$$

which gives

$$\frac{1}{r}\frac{\mathrm{d}}{\mathrm{d}r}\left(r \in_L (\alpha + \alpha_0) \frac{\mathrm{d}\theta}{\mathrm{d}r} \right) = -\frac{u_L q_R R \in_L}{\rho_L C_p \int_0^R u_L \in_L r \mathrm{d}r} \quad (17)$$

Taking temperature in terms of temperature difference with respect to wall and using relations Eqs. (14)–(16), the heat equation Eq. (17) can be written in the nondimensional form.Writing θ in dimensionless form as:

$$\frac{1}{r}\frac{\mathrm{d}}{\mathrm{d}r}\left(r \in_L (\alpha + \alpha_0) \frac{\mathrm{d}\theta^+}{\mathrm{d}r} \right) = -\frac{u_L R \in_L u^*}{\int_0^R u_L \in_L r \mathrm{d}r} \quad (18)$$

where $\theta^+ = \bar{\theta}/T^*$ and $T^* = (q/u^* \rho_L C_p)$.

Case 2. Center heating

Parameter A in Eq. (14) can be expressed in terms of imposed constant heat flux. Integrating over $r = m$ to R, where m is very small distance from center and represents a heat transfer element and using the fact that

$$q_C = -C_P \rho_L \in_L \alpha_0 \left(\frac{\mathrm{d}\theta}{\mathrm{d}r} \right)_m \ \text{ at } \ r = m$$
$$q_R = C_P \rho_L \in_L \alpha_0 \left(\frac{\mathrm{d}\theta}{\mathrm{d}r} \right)_R \ \text{ at } \ r = R \quad (19)$$

$$A = -\frac{q_c (R - m)}{\rho_L C_P \int_m^R u_L \in_L r \mathrm{d}r} \quad (20)$$

Using Eq. (14) and (20) and writing θ in dimensionless, gives

$$\frac{1}{r}\frac{\mathrm{d}}{\mathrm{d}r}\left(r \in_L (\alpha + \alpha_0) \frac{\mathrm{d}\theta^+}{\mathrm{d}r} \right) = -\frac{u_L (R - m) \in_L u^*}{\int_m^R u_L \in_L r \mathrm{d}r} \quad (21)$$

where $\theta^+ = \bar{\theta}/T^*$ and $T^* = (q/u^* \rho_L C_p)$.

The integral in the Eq. (18) and (21) was split into two parts, for up-flow region and for down-flow region. The up-flow integral was found to be positive and down-flow integral was negative. This ensures the sign of A to be positive in the central core and negative in the down-flow region.

5. Method of solution

The solution procedure consisted of two steps: the first step was to solve the momentum equations of gas, liquid

phases, turbulent kinetic energy (k) and turbulent energy dissipation rate (ε) (Eqs. (1)–(9) along with boundary condition Eq. (10)). The flow information obtained from the step one was used in step two: to obtain the value of heat transfer coefficient. For this purpose, Eq. (17) and (21) were solved by control volume technique of Patankar [8]. In the case of wall heating, a non-uniform grid (100 grids in region $0< r/R < 0.9$ and 900 grids in $0.9 < r/R < 1$) was used and for the case of center heating, a non-uniform grid (500 grids in region $0 < r/R < 0.055$, 100 grids in region $0.055 < r/R < 0.95$ and 500 grids in $0.95 < r/R < 1$) was used. The f_1, f_2, f_μ distribution was kept at the center as at wall, also the boundary condition for ε and k was given as that of wall for the case of center heating. The stepwise procedure used for getting the flow pattern is given in detail by Vitankar et al. [6].

6. Results and discussion

6.1. Comparison of the existing data and model predictions

There have been a large number of investigations on experimental measurement of heat transfer coefficient. A wide

Table 1
Heat transfer coefficient in bubble columns: summary of previous experimental work

Researcher	Gas–liquid system	Diameter/height (m)	Range of V_G (m s^{-1})	Sparger	Correlation
Fair et al. [9]	Air–water	0.457, 1.07	0.006–0.045	Sparge ring	$h_W = 8850 V_G^{0.22}$
Kast [10]	Air–water	0.288	0.025–0.06	Sieve plate, sintered nozzle, hole-type nozzle	$St = 0.1(Re\ Fr\ Pr^2)^{-0.22}$
Muller [11]	Air–water	0.09,0.19,0.29/1.2	0.004–0.12	Porous plate	Laminar $\{Nu = 750[Re^{0.292} Pr^{0.078} We^{-0.091} (D/L)^{0.1} (D/H_D)^{0.73}]\}$, Turbulent $\{Nu = 143[Re^{0.11} Pr^{0.078} We^{-0.091} (D/L)^{0.1} (D/H_D)^{0.73}]\}$
Ruckenstein and Smigelschi [12]	Air–water	–	0.01–0.2	28 Capillary tubes in the plate	$h_W = 0.28 k_L \left(\frac{g \bar{\epsilon}_G}{\nu}\right)^{1/3} \left(\frac{\nu}{\alpha}\right)^{1/3}$
Burkel [13]	Air–water	0.19	0.01–0.5	–	$St = 0.11(Re\ Fr\ Pr^{2.48})^{-0.23}$
Hart [14]	Air–water, air–ethylene glycol	0.099	0.003–0.2	1/4 inch. o.d. copper tube	$\frac{h_W}{\rho_L C_P V_G} \left(\frac{C_P \mu_L}{k_L}\right)^{0.6} = 0.125 \left(\frac{V_G^3 \rho_L}{\mu_L g}\right)^{-0.25}$
Steiff and Weinspach [15]	Air–water, air–silicone oil	0.19, 0.45, 0.7/2.1	0.004–0.2	–	$St = 0.113(Re\ Fr\ Pr^2)^{-0.26}$
Louisi [16]	Air–xylene, air–kogasene, air–decalin	0.1	–	–	$St = 0.136(Re\ Fr\ Pr^{1.94})^{-0.27}$
Joshi et al. [17]	Air–water	–	–	–	$\frac{h_W D}{k_L} = 0.087 \left(\frac{D^{1.33} g^{0.33} (V_G - \bar{\epsilon}_G V_{B\infty})^{0.33} \rho_L}{\mu_L}\right)^{0.8} \left(\frac{C_P \mu_L}{k_L}\right)^{0.33} \left(\frac{\mu_L}{\mu_w}\right)^{0.14}$
Deckwer [18]	Air–water	–	–	–	$St = 0.1(Re\ Fr\ Pr^2)^{-0.25}$
Hikita et al. [19]	Air–water, air–1-butanol, air–sucrose methanol	0.1, 0.19/1.62, 2.40	0.053–0.34	Single nozzle, nozzles—0.9, 1.3, 1.31, 2.06, 3.62 cm	$\frac{h_W}{\rho_L C_P V_G} \left(\frac{C_P \mu_L}{k_L}\right)^{2/3} = 0.411 \left(\frac{V_G \mu_L}{\sigma}\right)^{-0.851} \left(\frac{\mu_L^4 g}{\sigma \rho_L}\right)^{0.308}$
Lewis et al. [20]	Air–water, nitrogen–cumene, nitrogen–glycol	0.292	0.02–0.165	Perforated plates: 91 holes of 0.81 mm diameter	$h = \left[\frac{\delta}{k_L} + \left(\frac{\pi L_c}{4 k_L C_P \rho_L V_C}\right)^{1/2}\right]^{-1}$
Verma [21]	Air–water	0.108/1.7	0.1–0.4	Perforated plate: 91 holes of 0.81 mm	$\frac{h_W}{\rho_L C_P V_G} = 0.121(1 - \bar{\epsilon}_G) \left(\frac{C_P \mu_L}{k_L}\right)^{-0.5} \left(\frac{V_G^3 \rho_L}{\mu_L g}\right)^{-0.851}$
Yang et al. [22]	Compressed nitrogen-Paratherm NF heat transfer fluid	0.1016/1.37	0.01–0.25	Perforated plate with 120 square-pitched holes of 1.5 mm	$St = 0.2(Re\ Fr\ Pr^2)^{-0.25}$

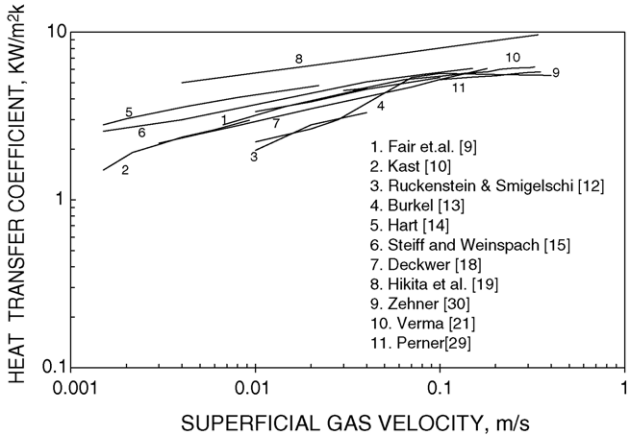

Fig. 2. Comparison of the correlations available in the published literature.

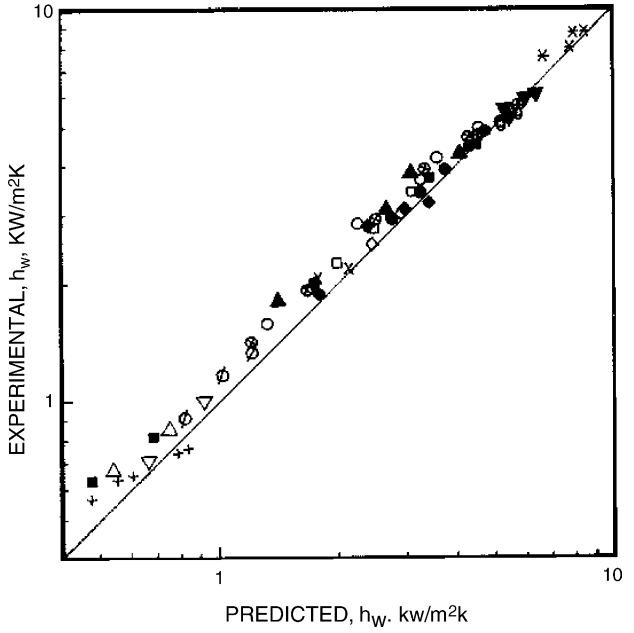

Fig. 3. Parity plot for the heat transfer correlation of Joshi et al. [17]. For other details refer Table 1. (●, ○) Fair et al. [9], (△) Muller [11], (◊) Ruckenstein and Smigelschi [12], (×) Burkel [13], (⊗, □) Hart [14], (△, Ø, ▽) Louisi [16], (◊) Deckwer [18], (*) Hikita et al. [19], (▽) Verma [21], (+) Yang et al. [22], (□) Perner [29], (θ) Zehner [30].

range of gas velocity, column diameter together with different gas–liquid and gas–liquid–solid systems have been studied in the published literature. A summary of these studies has been given in Table 1. The mechanism of heat exchange

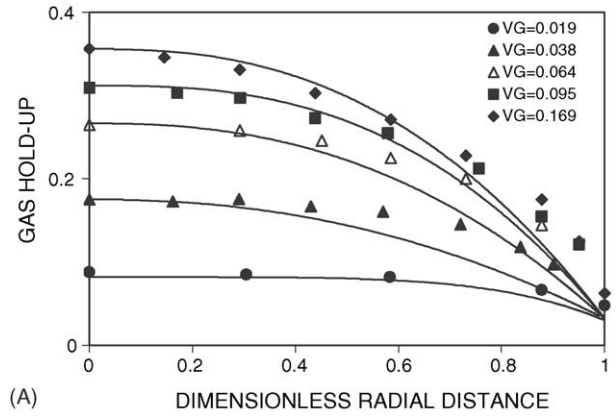

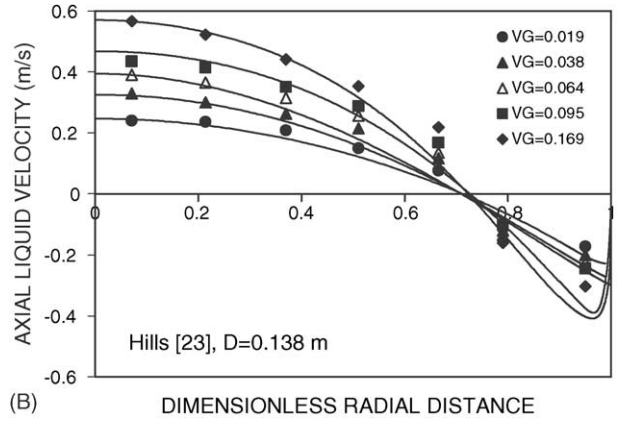

Fig. 4. Comparison between the low Reynolds number k–ε model predictions and the experimental data of Hills [23]. (A) Comparison of hold-up profiles, (B) comparison of liquid velocity profiles.

between two-phase dispersion and heat transfer area has also been discussed by several investigator and they have proposed heuristic models. Thus, it can be seen that the major effort has been on correlating the heat transfer data by means of empirical or semi-empirical correlations but the use of these expression is limited to the experimental conditions on which they are based. The constants involved in these correlations were determined to fit investigator's own data. In order to understand the comparative performance of these correlations, these have been plotted in the Fig. 2. The following observations were made by the analysis of the experimental data and the correlations shown in Fig. 2.

Table 2
Effect of diameter on flow and heat transfer coefficient

Diameter (m)	V_G (m s^{-1})	$\bar{\epsilon}_G$	m	C_B	Material balance		Energy balance[a]		V_C (m s^{-1})	Heat transfer coeff.
					C_0	C_1	RHS	LHS		
0.15	0.149 (0.15)[a]	0.219 (0.22)	3.4	0.5	2.2 (2.0)	0.33 (0.3)	1.13	1.10	0.38	5934.9
0.385	0.15 (0.15)	0.212 (0.22)	3.4	0.4	2.1 (2.0)	0.3 (0.3)	0.88	0.89	0.40	6192.0
1.0	0.154 (0.15)	0.215 (0.22)	3.4	0.2	2.5 (2.0)	0.32 (0.3)	0.95	1.08	0.48	6701.0
2.0	0.156 (0.15)	0.218 (0.22)	3.4	0.3	2.6 (2.0)	0.32 (0.3)	1.08	1.22	0.56	7005.0

[a] The bracketed numbers indicate the experimental values; LHS is volume integral of energy dissipation rate and RHS is Eq. (11).

Table 3
Effect of different gas–liquid system on flow and heat transfer coefficient

V_G (m s^{-1})	$\bar{\epsilon}_G$	C_B	Material balance		Energy balance[a]		V_S (m s^{-1})	Heat transfer coeff.
			C_0	C_1	RHS	LHS		
0.098 (0.1)	0.13 (0.128)	0.50	2.65 (2.8)	0.49 (0.5)	0.60	0.58	0.56	5398.52
0.106 (0.1)	0.16 (0.155)	0.47	2.35 (2.4)	0.41 (0.4)	0.57	0.55	0.51	4945.06
0.102 (0.1)	0.2 (0.2)	0.44	2.1 (2.0)	0.32 (0.3)	0.55	0.50	0.42	4643.12
0.105 (0.1)	0.23 (0.244)	0.41	1.5 (1.6)	0.28 (0.25)	0.56	0.48	0.37	4274.65

[a] The bracketed numbers indicate the experimental values; LHS is volume integral of energy dissipation rate and RHS is Eq. (11).

(i) For the same superficial gas velocity, the different investigators have observed different values of heat transfer coefficient. This may be due to the different gas hold-ups in the respective studies. It may be pointed out, at the same V_G the value of $\bar{\epsilon}_G$ depends upon the nature of gas–liquid system and the operating pressure and temperature. $\bar{\epsilon}_G$ further depends upon the sparger design and column height. $\bar{\epsilon}_G$ also depends upon the regime of operation (homogeneous or heterogeneous) which in turn depends upon V_G, D, sparger design, pressure, temperature, etc.

(ii) The heat transfer coefficient shows strong dependence on V_G at low superficial gas velocities ($V_G < 0.1$ m s^{-1}) and weaker dependence at higher superficial gas velocities.

(iii) Heat transfer is found to be independent of sparger design.

Table 4
Comparison between experimental and the CFD simulated values

Author	V_G (m s^{-1})	$\bar{\epsilon}_G$	Material balance		Energy balance[a]	
			C_0	C_1	LHS	RHS
Burkel [13]	0.018 (0.02)	0.052 (0.051)	1.98 (2.0)	0.31 (0.34)	0.038	0.032
	0.042 (0.04)	0.097 (0.095)	1.57 (2.0)	0.28 (0.34)	0.108	0.098
	0.058 (0.06)	0.127 (0.123)	2.1 (2.0)	0.315 (0.34)	0.187	0.142
	0.095 (0.10)	0.166 (0.169)	2.2 (2.0)	0.312 (0.34)	0.391	0.312
	0.142 (0.15)	0.234 (0.243)	1.89 (2.0)	0.312 (0.34)	0.761	0.658
	0.189 (0.2)	0.270 (0.265)	1.98 (2.0)	0.421 (0.34)	1.15	1.01
	0.241 (0.25)	0.290 (0.280)	2.11 (2.0)	0.289 (0.34)	1.55	1.26
	0.290 (0.30)	0.319 (0.180)	2.13 (2.0)	0.301 (0.34)	1.98	1.58
Steiff and Weinspach [15]	0.018 (0.02)	0.05 (0.045)	1.85 (2.0)	0.286 (0.3)	0.042	0.039
	0.039 (0.04)	0.105 (0.101)	1.75 (2.0)	0.298 (0.3)	0.113	0.112
	0.059 (0.06)	0.142 (0.141)	1.65 (2.0)	0.286 (0.3)	0.210	0.200
	0.079 (0.08)	0.173 (0.171)	2.15 (2.0)	0.295 (0.3)	0.320	0.312
	0.098 (0.10)	0.20 (0.191)	2.12 (2.0)	0.296 (0.3)	0.460	0.395
	0.14 (0.15)	0.25 (0.211)	1.89 (2.0)	0.356 (0.3)	0.860	0.865
	0.18 (0.20)	0.285 (0.272)	1.99 (2.0)	0.296 (0.3)	1.23	1.12
Hikita et al. [19]	0.068 (0.07)	0.14 (0.139)	2.12 (0.2)	0.31 (0.35)	0.23	0.20
	0.10 (0.10)	0.18 (0.174)	2.1 (0.2)	0.31 (0.35)	0.28	0.21
	0.176 (0.18)	0.25 (0.251)	1.9 (0.2)	0.35 (0.35)	0.51	0.45
	0.24 (0.24)	0.3 (0.293)	1.6 (0.2)	0.39 (0.35)	1.41	1.30
	0.34 (0.35)	0.35 (0.34)	1.54 (0.2)	0.38 (0.35)	1.77	1.62
Lewis et al. [20]	0.035 (0.04)	0.097 (0.098)	3.12 (3.45)	0.21 (0.25)	0.119	0.112
	0.053 (0.054)	0.123 (0.121)	3.12 (3.45)	0.125 (0.25)	0.2019	0.210
	0.067 (0.068)	0.140 (0.135)	2.15 (3.45)	0.215 (0.25)	0.295	0.251
	0.076 (0.08)	0.152 (0.157)	2.95 (3.45)	0.214 (0.25)	0.381	0.315
	0.101 (0.105)	0.171 (0.177)	2.95 (3.45)	0.29 (0.25)	0.575	0.517
	0.135 (0.143)	0.192 (0.19)	2.89 (3.45)	0.245 (0.25)	0.893	0.785
	0.162 (0.163)	0.201 (0.192)	2.56 (3.45)	0.198 (0.25)	1.067	0.997
Verma [21]	0.031 (0.035)	0.083 (0.081)	2.15 (2.0)	0.39 (0.35)	0.14	0.12
	0.051 (0.05)	0.111 (0.110)	2.5 (2.0)	0.32 (0.35)	0.16	0.16
	0.097 (0.1)	0.179 (0.18)	1.95 (2.0)	0.35 (0.35)	0.30	0.31
	0.20 (0.20)	0.259 (0.26)	1.64 (2.0)	0.39 (0.35)	0.45	0.37
	0.25 (0.25)	0.289 (0.29)	1.82 (2.0)	0.36 (0.35)	0.51	0.48
	0.32 (0.35)	0.333 (0.311)	1.58 (2.0)	0.34 (0.35)	0.65	0.64

[a] The bracketed numbers indicate the experimental values; LHS is volume integral of energy dissipation rate and RHS is Eq. (11).

(iv) For column diameter greater than 0.19 m, heat transfer coefficient becomes independent of the column diameter.

In view of the above observations, Joshi et al. [17] included the effect of $\bar{\epsilon}_G$ on the flow pattern and the average liquid circulation velocity. They also included the above observations in their correlation. This correlation has been compared with all published experimental data and the average deviation was found to be 8% (Fig. 3). In view of this, it was thought desirable to develop a CFD model for flow and heat transfer in bubble column.

6.2. Present CFD model for flow and heat transfer

As a first step, it is important to establish the validity of the model for flow pattern. Therefore, comparison has been made with the experimental data of Hills [23], Nottenkamper et al. [24], Menzel et al. [25], Yao et al. [26], Yu and Kim [27] and Grienberger and Hoffman [28] and details are given in Vitankar et al. [6]. The excellent agreement was obtained between the model predictions and the experimental measurements. For instance, Fig. 4 shows a typical case of such comparison. The agreement between the predicted and the experimental profiles of axial velocity can be seen to be excellent. It may be pointed out such an agreement has been obtained over a wide range of column diameter, superficial gas and liquid velocities as covered by the above-mentioned authors.

In view of the above-mentioned favorable comparison, it was thought desirable to extend model for the analysis of heat transfer process in the bubble column. It was assumed that the eddy diffusivities for momentum and heat are equal. The analysis was carried out for both cases of location of heating element, i.e., center and at wall position. The resulting temperature profile was used for the calculation of heat transfer coefficient using the following equation:

$$q = h_W \, \Delta\bar{\theta} \tag{22}$$

normalising $\Delta\bar{\theta}$ by T^* $(=q/u^* \rho_L C_p)$,

$$h_W = \frac{\rho_L C_P u^*}{\Delta\theta^+} \tag{23}$$

6.3. Effect of column diameter

Diameter has considerable effect on the performance of the bubble column. The effect of diameter (D) on flow variables and heat transfer coefficient has been systematically investigated. It can be seen from Table 2 that with an increase in diameter from 0.15 to 2.0 m, a significant increase in the magnitude of the liquid velocity occurs. Diameter seems to have slight effect on the heat transfer coefficient. It can be seen from the Table 2 that with a reduction in diameter from 2.0 to 0.15 m, heat transfer coefficient reduces by 15%.

6.4. Effect of gas–liquid system

The major influence of physical properties is basically on the average bubble size and bubble rise velocity. The other factors, which influence d_B and V_S, are the sparger design and the energy dissipation rate. The sparger loses influence when H_D/D ratio is greater than a critical number depending upon the coalescing nature of gas–liquid system. Therefore, for given V_G, the value of V_S can be considered as a signatory representative of all the physical properties including nature of gas–liquid system. Therefore, effect of physical properties was investigated by considering V_S over a wide range. It has been emphasized earlier that the accurate prediction of V_S for an unknown gas–liquid system is very difficult with the present status of knowledge. Therefore, we have recommended the measurements of C_0 and C_1 for a given system. This means that any gas–liquid system is a set of C_0 and C_1. The simulations have been carried out for four different sets of C_0, C_1 for superficial gas velocity of 0.1 m s^{-1}. It can be seen that as the slip velocity increases (correspondingly C_1 increases), the gas phase residence time and the average hold-up $\bar{\epsilon}_G$ reduces. It can be concluded from the Table 3 that with change in C_0 and C_1, from ($C_0 = 1.6$, $C_1 = 0.25$) to ($C_0 = 2.8$, $C_1 = 0.5$), heat transfer coefficient increases by 25%.

6.5. Comparison of heat transfer data with the experimental data

The simulations were carried out for case of center heating and wall heating. The model predictions have been compared with the experimental data of Burkel [13], Steiff and Weinspanch [15] and Hikita et al. [19] for the case of wall heating and Lewis et al. [20] and Verma [21] for second case of center heating. The results have been given in Table 4 and

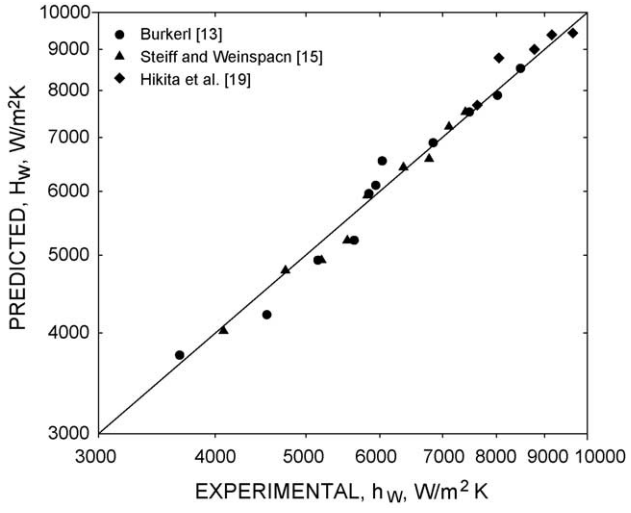

Fig. 5. Parity plot between the predicted heat transfer coefficient and the experimental data of Burkel [13], Steiff and Weinspach [15], Hikita et al. [19] for the case of wall heating.

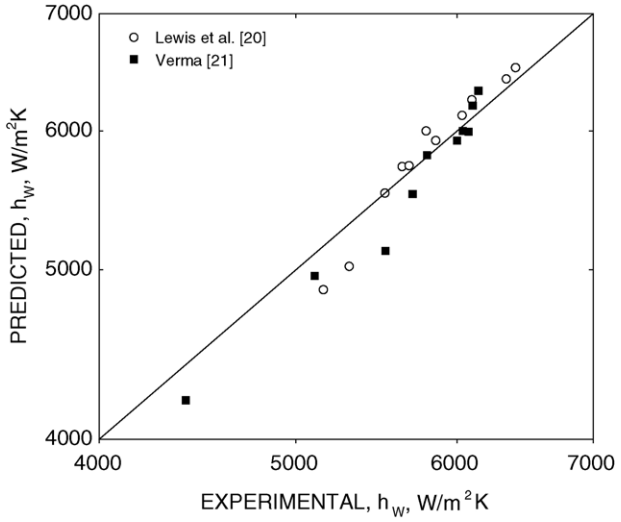

Fig. 6. Parity plot between the predicted heat transfer coefficient and the experimental data of Lewis et al. [20] and Verma [21] for the case of central heating.

the parity plot for heat transfer coefficient in Figs. 5 and 6, which show an excellent agreement between the CFD predictions and the experimental measurements.

7. Conclusions

(1) In this work, for the predictions of flow pattern, the knowledge of hold-up profile has not been assumed to be available. This aspect may be considered as a significant step forward in the development of predictive procedures for flow pattern in bubble columns.

(2) A stepwise procedure has been developed for the prediction of hold-up and liquid phase velocity profiles as well as slip velocity. An excellent agreement between the predicted and the experimental profiles of hold-up and axial velocity was observed over a wide range of column diameter $0.138 < D < 0.6$ m and superficial gas velocity $0.01 < V_G < 1.452$ m s^{-1}. These data have been reported from different laboratories by Hills [23], Nottenkamper [24], Menzel et al. [25], Yao et al. [26], Yu and Kim [27] and Grienberger and Hofmann [28] and practically cover all the published information.

(3) A low Reynolds number model has been developed for the analysis of heat transfer near wall as well as at centre. A very good agreement was found between the predicted and the experimental values of heat transfer coefficient.

References

[1] H.B. Stewart, B. Wendroff, Two-phase flow: models and methods, J. Comp. Phy. 56 (1984) 363–409.
[2] H.A. Jakobsen, B.H. Sannaes, S. Grevskott, H.F. Svendsen, Modelling of vertical bubble-driven flows, Ind. Eng. Chem. Res. 36 (1997) 4052–4074.
[3] J.B. Joshi, Computational flow modeling and design of bubble column reactors, Chem. Eng. Sci. 56 (2001) 5893–5933.
[4] S.S. Thakre, J.B. Joshi, CFD modeling of heat transfer in turbulent pipe flows, A. I. Ch. E. J. 46 (2000) 1798–1812.
[5] Y.G. Lai, R.M.C. So, On near wall turbulent flow modeling, J. Fluid Mech. 221 (1990) 641–673.
[6] V.S. Vitankar, M.T. Dhotre, J.B. Joshi, A low Reynolds number k–ε model for the prediction of flow pattern and pressure drop in bubble column reactors, Chem. Eng. Sci. 57 (2002) 3235–3250.
[7] T.J. Lin, S.P. Wang, Effects of macroscopic hydrodynamics on heat transfer in bubble columns, Chem. Eng. Sci. 56 (2001) 1143–1149.
[8] S.V. Patankar, Numerical Heat Transfer and Fluid Flow, McGraw-Hill, New York, 1980.
[9] J.R. Fair, A.J. Lambright, J.W. Anderson, Heat transfer in sparged contactors, Ind. Eng. Chem. Proc. Des. Dev. 1 (1962) 33–36.
[10] W. Kast, Analyse des warmeubergangs in blasensaulen, Int. J. Heat Mass Transfer 5 (1962) 329–336.
[11] D. Muller, Dr. Ing. Thesis, TU Berlin, 1962.
[12] E. Ruckenstein, O. Smigelschi, Heat transfer to bubble beds, Trans. Inst. Chem. Eng 43 (1965) T334–T338.
[13] W. Burkel, Dr. Ing. Thesis, TU Munchen, 1974.
[14] W.F. Hart, Heat transfer in bubble agitated system, Ind. Eng. Chem. Proc. Des. Dev. 15 (1976) 109–144.
[15] A. Stieff, P.M. Weinspach, Heat transfer in stirred and non-stirred gas liquid reactors, Ger. Chem. Eng. 1 (1978) 150–161.
[16] Y. Louisi, Dr. Ing. Thesis, TU Berlin, 1979.
[17] J.B. Joshi, M.M. Sharma, Y.T. Shah, C.P.P. Singh, M. Ally, G.E. Klinzing, Heat transfer in multiphase contactors, Chem. Eng. Comm. 6 (1980) 257–271.
[18] W.D. Deckwer, On the mechanism of heat transfer in bubble column reactors, Chem. Eng. Sci. 35 (1980) 1341–1346.
[19] H. Hikita, S. Asai, H. Kikukawa, T. Zalke, M. Ohue, Heat transfer coefficient in bubble columns, Ind. Eng. Chem. Proc. Des. Dev. 20 (1981) 540–545.
[20] D.A. Lewis, R.W. Field, A.M. Xavier, D. Edwards, Heat transfer in bubble columns, Trans. Inst. Chem. Eng. 60 (1982) 40–47.
[21] A.K. Verma, Mechanism of heat transfer in bubble column, Chem. Eng. J. 42 (1989) 205–208.
[22] Q.G. Yang, X. Luo, R. Lau, L.S. Fan, Heat transfer characteristics in slurry bubble columns at elevated pressures and temperatures, Ind. Eng. Chem. Res. 39 (2000) 2568–2577.
[23] J.H. Hills, Radial non-uniformity of velocity and voidage in a bubble column, Trans. Inst. Chem. Eng. 52 (1974) 1–9.
[24] R. Nottenkamper, A. Stieff, P.M. Weinspach, Experimental investigations of hydrodynamics of bubble columns, Ger. Chem. Eng. 6 (1983) 147–155.
[25] T. Menzel, T. Weide, O. Staudacher, O. Wein, U. Onken, Reynolds shear stress for modelling of bubble column reactor, Ind. Eng. Chem. Res. 29 (1990) 988–994.
[26] B.P. Yao, C. Zheng, H.E. Gasche, H. Hofmann, Bubble behaviour and flow structure of bubble columns, Chem. Eng. Proc. 29 (1991) 65–75.
[27] Y.H. Yu, S.D. Kim, Bubble properties and local liquid velocity in the radial direction of co-current gas–liquid flow, Chem. Eng. Sci. 46 (1991) 313–320.
[28] J. Grienberger, H. Hofmann, Investigation and modeling of bubble columns, Chem. Eng. Sci. 47 (1992) 2215–2220.
[29] D. Perner, Dipl. Arbeit, TU Berlin, 1960.
[30] P. Zehner, Momentum, mass and heat transfer in bubble columns. Part 2. Axial blending and heat transfer, Inter. Chem. Eng. 20 (1986) 29–35.